Int. J. Solids Structures Vol. 30, No. 21, pp. 2911–2928, 1993
Printed in Great Britain

0020–7683/93 $6.00+.00

INTERLAMINAR STRESSES IN A CENTRALLY NOTCHED COMPOSITE LAMINATE

M.-H. R. JEN, Y. S. KAU and J. M. HSU
Department of Mechanical Engineering, National Sun Yat-Sen University, Kaohsiung, Taiwan 80424, R.O.C.

(*Received* 2 *January* 1993; *in revised form* 8 *April* 1993)

Abstract—A plane stress solution for an anisotropic plate with a circular hole, developed by Savin, is extended to derive the interlaminar stresses in a centrally notched composite laminate under uniform tension. Based upon Lekhnitskii's stress potentials, theory of anisotropic elastic body and boundary layer effect, stress shapes are chosen such that the zeroth order equilibrium equations, interface continuity and boundary conditions are satisfied. The unknown parameters in the stress expressions are then determined by the requirement of stress integral equilibrium. The merit of our model is highlighted by obtaining the interlaminar stresses and the order of boundary layer stress singularity simultaneously. Several examples of $[0/90]_s$, $[\pm 45]_s$ and $[0/90/\pm 45]_s$ graphite/epoxy composite laminates containing centrally circular holes are analysed.

NOMENCLATURE

A_i	constant
a_{ij}	stiffness matrix element
B_i	constant
b_{ij}	flexibility matrix element
D_i	operator
F	Airy stress function
h	laminate thickness
k	ply number
m	number of plies in half laminate
n	parameter
P_{kl}, Q_{kl}	stress function
R	hole radius
r	coordinate
S_{ij}	reduced stiffness
T_i	ith ply thickness
x, y, z	coordinates
z_i	$x+\mu_i y$
α	parameter
$\alpha_{1,2}$	real constants
$\beta_{1,2}$	real constants
λ	parameter
ρ, η, δ	dimensionless variable
ε	strain
μ_i	root of flexibility equation
$\phi_{1,2}$	stress functions
σ_0	uniform extension stress at far field
σ^0	zeroth order stress
σ_{ij}	stress
θ	coordinate.

1. INTRODUCTION

Because of the mismatch in elastic properties between plies, the composite laminate under in-plane loading develops serious interlaminar stresses in the boundary-layer regions close to the free edges. When the magnitude of interlaminar stresses becomes large enough, delamination may occur and failure may follow. It is obvious that the Classical Laminated Plate Theory (CLPT) is not valid for interlaminar problems and thus methods for three-dimensional stresses are required. Many investigators have made some attempts to calculate the interlaminar stresses at straight free edges since 1970 (Pipes and Pagano, 1970). These methods include finite difference by Pipes and Pagano (1970), finite element by Rybicki and Schmueser (1976), Wang and Crossman (1977), Spilker and Chou (1980), and eigenfunction

expansions by Wang and Choi (1982a, b). But, only a limited number of papers have been proposed for interlaminar stresses at curved edges in composite laminates (Rybicki and Schmueser, 1976; Tang, 1977; Ye and Yang, 1988; Zhang and Ueng, 1988; Lucking *et al.*, 1984; Carlsson, 1983; Ericson *et al.*, 1984). From a literature survey, we find that finite element and finite difference methods require a large amount of computer storage and computer time. The eigenfunction method involves a complicated and tedious eigenvalue problem solution. Hence, the drawbacks make these methods restricted to deal with interlaminar stresses around the free edge of a circular hole in a composite laminate.

Generally speaking, the published papers may be categorized into (a) computing the interlaminar stresses at straight free edges, (b) obtaining interlaminar stresses at curve edges, and (c) obtaining the singularity order at straight free edges and interlaminar stresses as well. To the best of our knowledge, very little research work has been reported to yield singularity and interlaminar stresses simultaneously until now. The present solution method, based on Lekhnitskii's stress potentials, theory of anisotropic elastic body, boundary layer effect and stress integral equilibrium, attempts to give a more accurate approximation to the three-dimensional stresses in a notched composite laminate. This method also has the ability to analyse the order of singularity of boundary-layer stress. Thus, the proposed method herein has the advantage of being able to solve the interlaminar stresses between any two plies and for all directions. It is also an efficient technique for the designer to avoid delamination for the pronely delaminated composites.

2. FORMULATION

First, a cylindrical coordinate system for the notched laminate, i.e. r, θ, z, is introduced as shown in Fig. 1. A uniform tensile stress σ_0 is applied at both ends. The laminate is composed of $2m$ plies, with a thickness of h. It has a centrally circular hole of radius R. The origin of the coordinate system is located at the center of the hole on the midplane, while the z-axis is perpendicular to the plane of laminate.

Next, the dimensionless variables are defined as follows:

$$\rho = \frac{r-R}{h},$$

$$\eta = \frac{z}{h},$$

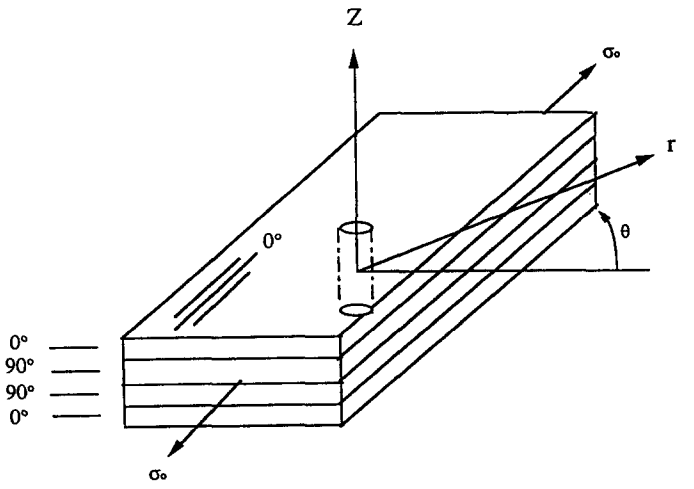

Fig. 1. The geometry of a centrally notched laminate.

$$\delta = \frac{h}{R}.$$

If the body forces are neglected, the equilibrium equations (Reiss, 1961), are

$$\sigma_{rz,\eta} + \left[\sigma_{rr,\rho} + \frac{\delta}{1+\rho\delta}(\sigma_{r\theta,\theta} + \sigma_{rr} - \sigma_{\theta\theta})\right] = 0,$$

$$\sigma_{z\theta,\eta} + \left[\sigma_{r\theta,\rho} + \frac{\delta}{1+\rho\delta}(\sigma_{\theta\theta,\theta} + \sigma_{r\theta})\right] = 0,$$

$$\sigma_{zz,\eta} + \left[\sigma_{rz,\rho} + \frac{\delta}{1+\rho\delta}(\sigma_{z\theta,\theta} + \sigma_{rz})\right] = 0. \tag{1}$$

By means of asymptotic expansions, the boundary layer stresses may be expressed in a power series of δ, that is

$$\sigma = \sum_{n=0}^{\infty} \sigma^n \delta^n, \tag{2}$$

where σ^n are denoted as the boundary-layer stress coefficients, δ is very small near the free edge and δ^n becomes much smaller for $n > 0$. Substituting eqn (2) into eqn (1) and neglecting the higher order terms of δ (Tang, 1977), yields the zeroth order equilibrium equations

$$\sigma^0_{rz,\eta} + \sigma^0_{rr,\rho} = 0,$$
$$\sigma^0_{\theta z,\eta} + \sigma^0_{r\theta,\rho} = 0,$$
$$\sigma^0_{zz,\eta} + \sigma^0_{rz,\rho} = 0. \tag{3}$$

These boundary layer equations are the same as those adopted by Pipes and Pagano (1970).

It is assumed that for each stress, except $\sigma_{\theta\theta}$, the dependence on r and z can be functionally separated (Kassapoglou and Lagace, 1986). These stresses in the kth ply of a $2m$-ply laminate can thus be presented as:

$$\sigma^{0(k)}_{kl} = P^{(k)}_{kl}(\rho) Q^{(k)}_{kl}(\eta) \quad kl = rr, r\theta, rz, \theta z, zz. \tag{4}$$

Substituting eqn (4) into eqn (3), we have

$$Q^{(k)}_{rr} = \frac{\partial Q^{(k)}_{rz}}{\partial \eta}, \quad Q^{(k)}_{rz} = \frac{\partial Q^{(k)}_{zz}}{\partial \eta}, \quad Q^{(k)}_{r\theta} = \frac{\partial Q^{(k)}_{\theta z}}{\partial \eta},$$

$$P^{(k)}_{rz} = -\frac{\partial P^{(k)}_{rr}}{\partial \rho}, \quad P^{(k)}_{zz} = -\frac{\partial P^{(k)}_{rz}}{\partial \rho}, \quad P^{(k)}_{\theta z} = -\frac{\partial P^{(k)}_{r\theta}}{\partial \rho}. \tag{5}$$

It is obvious from eqn (5) that only four stress functions, i.e. $Q^{(k)}_{rr}$, $Q^{(k)}_{r\theta}$, $P^{(k)}_{rr}$ and $P^{(k)}_{r\theta}$ must be assumed as stress functions of $P^{(k)}_{kl}$ and $Q^{(k)}_{kl}$, and the remaining six stress functions $Q^{(k)}_{rz}$, $Q^{(k)}_{\theta z}$, $Q^{(k)}_{zz}$, $P^{(k)}_{rz}$, $P^{(k)}_{\theta z}$ and $P^{(k)}_{zz}$ can then be determined.

Considering the $Q^{(k)}_{kl}$ function first, we find that the in-plane stresses $\sigma^{(k)}_{rr}$, $\sigma^{(k)}_{r\theta}$ are constant in a given ply. This implies that both stresses do not vary along the z-axis in a certain ply and the simplest forms for $Q^{(k)}_{rr}(\eta)$ and $Q^{(k)}_{r\theta}(\eta)$ can be specified as:

$$Q_{rr}^{(k)}(\eta) = 1,$$
$$Q_{r\theta}^{(k)}(\eta) = 1. \tag{6}$$

From eqn (5) the remaining three functions can be obtained:

$$Q_{rz}^{(k)}(\eta) = \eta + B_1^{(k)},$$
$$Q_{zz}^{(k)}(\eta) = \tfrac{1}{2}\eta^2 + B_1^{(k)}\eta + B_2^{(k)},$$
$$Q_{\theta z}^{(k)}(\eta) = \eta + B_3^{(k)}, \tag{7}$$

where $B_1^{(k)}$, $B_2^{(k)}$ and $B_3^{(k)}$ are constants to be determined by interface continuity. Equations (6) and (7) are the basic expressions for $Q_{kl}^{(k)}(\eta)$ functions.

To consider singularity behavior, $P_{kl}^{(k)}(\rho)$ are chosen to be a combination of power functions in ρ. A shape for $P_{rr}^{(k)}(\rho)$ is assumed by Jen (1992) as,

$$P_{rr}^{(k)}(\rho) = A_1^{(k)}\rho^{\alpha} + A_2^{(k)}\rho^{\alpha\lambda} + A_3^{(k)}\,\mathrm{e}^{-\alpha\lambda\rho}, \tag{8}$$

where $A_1^{(k)}$, $A_2^{(k)}$, $A_3^{(k)}$ and λ, α are unknown constants to be determined. The adoption of the form in eqn (8) is motivated by the stress variation and boundary conditions of σ_{rr} around the hole edge reported by Savin (1968). The constants $A_i^{(k)}$ are involved in the boundary conditions of boundary layer stress. λ, α are dimensionless and can be calculated from stress integral equilibrium equations. Similarly, the $P_{r\theta}^{(k)}(\rho)$ function can also be assumed as

$$P_{r\theta}^{(k)}(\rho) = A_4^{(k)}\rho^{\alpha-1} + A_5^{(k)}\,\mathrm{e}^{-\alpha\rho}. \tag{9}$$

Then the remaining $P_{kl}^{(k)}(\rho)$ functions can be derived from eqn (5) as

$$P_{zz}^{(k)}(\rho) = A_1^{(k)}\alpha(\alpha-1)\rho^{\alpha-2} + A_2^{(k)}(\lambda\alpha-1)\lambda\alpha\rho^{\lambda\alpha-2} + A_3^{(k)}\alpha^2\lambda^2\,\mathrm{e}^{-\alpha\lambda\rho},$$
$$P_{rz}^{(k)}(\rho) = -A_1^{(k)}\alpha\rho^{\alpha-1} - A_2^{(k)}\lambda\alpha\rho^{\lambda\alpha-1} + A_3^{(k)}\lambda\alpha\,\mathrm{e}^{-\alpha\lambda\rho},$$
$$P_{\theta z}^{(k)}(\rho) = -A_4^{(k)}(\alpha-1)\rho^{\alpha-2} + A_5^{(k)}\alpha\,\mathrm{e}^{-\alpha\rho}. \tag{10}$$

3. STRESS ANALYSIS

Suppose that each ply has the same in-plane stresses in the entire laminate except for the area around the hole edge extending to a small distance. In this small region, different plies possess varied high stresses because of the free boundary effect and significant interlaminar stresses existing in this region. The determination of stress field in a composite laminate with a hole under in-plane loading can be divided into two parts. One is the in-plane stress dominating field predicted by plane stress solution, another is the boundary layer stress field in the boundary layer region. Since interlaminar stresses will arise in any medium with layers of varying elastic constants if an in-plane gradient exists in the stress field, it is known to us that a significant in-plane gradient occurs in the boundary layer region according to many reports (Rybicki and Schmueser, 1976; Wang and Crossman, 1977; Spilker and Chou, 1980; Wang and Choi, 1982a, b; Tang, 1977). Hence, it is reasonable to assume that interlaminar stresses exist in this region. In the case of an anisotropic plate with a circular hole subjected to a uniform tensile load σ_0 along one of the principal material directions, the compatibility equation may be expressed (Lekhnitskii, 1963) as

$$b_{22}\frac{\partial^4 F}{\partial x^4} - 2b_{26}\frac{\partial^4 F}{\partial x^3\,\partial y} + (2b_{12}+b_{66})\frac{\partial^4 F}{\partial x^2\,\partial y^2} - 2b_{16}\frac{\partial^4 F}{\partial x\,\partial y^3} + b_{11}\frac{\partial^4 F}{\partial y^4} = 0, \tag{11}$$

where F is the Airy stress function (Timoshenko and Goodier, 1951), b_{ij} are the elements

of the flexibility matrix, referring to Appendix A. However, eqn (11) can be decomposed into four differential operators of the first order, and then it has the form

$$D_4D_3D_2D_1F = 0, \tag{12}$$

where

$$D_k = \frac{\partial}{\partial y} + \mu_k \frac{\partial}{\partial x} \quad \text{and } \mu_k$$

are the roots of the corresponding algebraic equation

$$b_{11}\mu^4 - 2b_{16}\mu^3 + (2b_{12}+b_{66})\mu^2 - 2b_{26}\mu + b_{22} = 0. \tag{13}$$

Lekhnitskii (1968) proved that the numbers of μ_k are always complex or purely imaginary. Two of these numbers are conjugates of the remaining two. These parameters are denoted as

$$\mu_1 = \alpha_1 + i\beta_1, \quad \mu_2 = \alpha_2 + i\beta_2, \quad \mu_3 = \alpha_1 - i\beta_1, \quad \mu_4 = \alpha_2 - i\beta_2,$$

where α_1, α_2, β_1 and β_2 are real constants.

The plane stress expressions can be written in terms of the two stress functions $\phi_1(z_1)$ and $\phi_2(z_2)$ (Savin, 1968; Lekhnitskii, 1963), as

$$\begin{aligned}
\sigma_x^p &= \sigma_0 + 2\,\mathrm{Re}\,[\mu_1^2\phi_1'(z_1) + \mu_2^2\phi_2'(z_2)],\\
\sigma_y^p &= 2\,\mathrm{Re}\,[\phi_1'(z_1) + \phi_2'(z_2)],\\
\sigma_{xy}^p &= -2\,\mathrm{Re}\,[\mu_1\phi_1'(z_1) + \mu_2\phi_2'(z_2)],
\end{aligned} \tag{14}$$

where

$$\phi_1(z_1) = \frac{-\sigma_0 R^2(i+\mu_1)}{2(\mu_1-\mu_2)\{z_1 + [z_1^2 - R^2(1+\mu_1^2)]^{1/2}\}},$$

$$\phi_2(z_2) = \frac{\sigma_0 R^2(i+\mu_2)}{2(\mu_1-\mu_2)\{z_2 + [z_2^2 - R^2(1+\mu_2^2)]^{1/2}\}},$$

$z_1 = x+\mu_1 y$, $z_2 = x+\mu_2 y$, and R is the radius of the circular hole.

In eqn (14) the superscripts p represent the plane stresses associated with the laminate. The stresses at each individual layer may be found from the following constitutive equations for each layer:

$$\{\sigma_i^p\}^k = [S_{ij}]^k\{\varepsilon_j\}, \tag{15}$$

where $\{\sigma_i^p\}^k$ represent the plane stresses in the kth layer, and k is the layer number. S_{ij} illustrate the terms of reduced stiffness. For the entire laminate, the strain field can be calculated from the stress–strain relationship.

3.1. *Determination of* P_{kl}

The boundary conditions for the boundary region in the kth ply are:

$$\begin{aligned}
&\text{at } r = R, \quad \sigma_{rr}^{0(k)} = \sigma_{rr}^{p(k)}, \quad \sigma_{rz}^{0(k)} = 0, \quad \sigma_{r\theta}^{0(k)} = \sigma_{r\theta}^{p(k)},\\
&\text{at } r = R+nh, \quad \sigma_{rr}^{0(k)} = \sigma_{rr}^{0p(k)}, \quad \sigma_{rz}^{0(k)} = 0, \quad \sigma_{r\theta}^{0(k)} = \sigma_{r\theta}^{0p(k)},
\end{aligned} \tag{16}$$

where nh is the distance of the boundary layer from the hole edge, and it is dependent on

many factors. For a specific lamination and loading condition, it depends primarily on the geometric ratio, i.e. R/h. Generally speaking, the thicker the laminate is, the larger the boundary layer width will become. For the laminates studied here, $0 < n < 2$ is large enough to encompass all possibilities. Some reports reveal the same results (Tang, 1977; Lucking *et al.*, 1984). In eqn (16) σ_{ij}^{p} are the plane stresses at the hole edge and σ_{ij}^{0p} are the plane stresses at a distance of nh from the hole edge obtained by eqn (15). The proper choice of n will be discussed in the next section. Substituting the boundary conditions of eqn (16) into eqns (8) and (9), we obtain the constants $A_i^{(k)}$:

$$A_1^{(k)} = -\frac{\lambda\sigma_{rr}^{0p(k)}}{n^{\alpha}(1-\lambda)}, \quad A_2^{(k)} = \frac{\sigma_{rr}^{0p(k)}}{n^{\alpha\lambda}(1-\lambda)}, \quad A_3^{(k)} = \sigma_{rr}^{p(k)}, \quad A_4^{(k)} = \frac{\sigma_{r\theta}^{0p(k)}}{n^{\alpha-1}}, \quad A_5^{(k)} = \sigma_{r\theta}^{p(k)}.$$

Thus $P_{kl}^{(k)}(\rho)$ can be computed by substitution of $A_1^{(k)}$ to $A_5^{(k)}$ into eqns (8)–(10); they are

$$P_{rr}^{(k)} = \frac{\sigma_{rr}^{0p(k)}}{1-\lambda}\left[\left(\frac{r-R}{nh}\right)^{\lambda\alpha} - \lambda\left(\frac{r-R}{nh}\right)^{\alpha}\right] + \sigma_{rr}^{p(k)} \exp\left(-\alpha\lambda\left(\frac{r-R}{h}\right)\right),$$

$$P_{r\theta}^{(k)} = \sigma_{r\theta}^{0p(k)}\left(\frac{r-R}{nh}\right)^{\alpha-1} + \sigma_{r\theta}^{p(k)} \exp\left(-\alpha\left(\frac{r-R}{h}\right)\right),$$

$$P_{rz}^{(k)} = -\frac{\lambda\alpha\sigma_{rr}^{0p(k)}}{n(1-\lambda)}\left[\left(\frac{r-R}{nh}\right)^{\lambda\alpha-1} - \left(\frac{r-R}{nh}\right)^{\alpha-1}\right] + \sigma_{rr}^{p(k)}\alpha\lambda \exp\left(-\alpha\lambda\left(\frac{r-R}{h}\right)\right),$$

$$P_{\theta z}^{(k)} = -\frac{(\alpha-1)\sigma_{r\theta}^{0p(k)}}{n}\left(\frac{r-R}{nh}\right)^{\alpha-2} + \sigma_{r\theta}^{(k)}\alpha \exp\left(-\alpha\left(\frac{r-R}{h}\right)\right),$$

$$P_{zz}^{(k)} = \frac{\lambda\alpha\sigma_{rr}^{0p}}{n^2(1-\lambda)}\left[(\lambda\alpha-1)\left(\frac{r-R}{nh}\right)^{\lambda\alpha-2} - (\alpha-1)\left(\frac{r-R}{nh}\right)^{\alpha-2}\right] + \sigma_{rr}^{p(k)}\alpha^2\lambda^2 \exp\left(-\alpha\lambda\left(\frac{r-R}{h}\right)\right). \tag{17}$$

3.2. *Determination of* Q_{kl}

The functions $Q_{kl}^{(k)}$ are determined from the stress continuity condition at ply interfaces. Consider the interface between ply k and ply $k+1$, the following stress continuity conditions are imposed:

$$\sigma_{ij}^{0(k+1)}(z^{(k+1)} = T_{k+1}) = \sigma_{ij}^{0(k)}(z^{(k)} = 0), \tag{18}$$

where $z^{(k)}$ is measured locally from the bottom of the corresponding ply. T_{k+1} is the thickness of the corresponding ply. Starting from the bottom surface of the laminate and proceeding up the midplane, we find that the constants $B_i^{(k)}$ are dependent on the values of B_i of all plies below that particular kth ply.

The continuity conditions for σ_{rz} are

$$0 = \left\{\frac{-\lambda\alpha\sigma_{rr}^{0p(m)}}{n(1-\lambda)}\left[\left(\frac{r-R}{nh}\right)^{\lambda\alpha-1} - \left(\frac{r-R}{nh}\right)^{\alpha-1}\right] + \sigma_{rr}^{p(m)}\alpha\lambda \exp\left(-\alpha\lambda\left(\frac{r-R}{h}\right)\right)\right\}\{0 + B_1^{(m)}\},$$

$$\left\{\frac{-\lambda\alpha\sigma_{rr}^{0p(m)}}{n(1-\lambda)}\left[\left(\frac{r-R}{nh}\right)^{\lambda\alpha-1} - \left(\frac{r-R}{nh}\right)^{\alpha-1}\right] + \sigma_{rr}^{p(m)}\alpha\lambda \exp\left(-\alpha\lambda\left(\frac{r-R}{h}\right)\right)\right\}\left\{\frac{T_m}{h} + B_1^{(m)}\right\}$$

$$= \left\{\frac{-\lambda\alpha\sigma_{rr}^{0p(m-1)}}{n(1-\lambda)}\left[\left(\frac{r-R}{nh}\right)^{\lambda\alpha-1} - \left(\frac{r-R}{nh}\right)^{\alpha-1}\right] + \sigma_{rr}^{p(m-1)}\alpha\lambda \exp\left(-\alpha\lambda\left(\frac{r-R}{h}\right)\right)\right\}\{0 + B_1^{(m-1)}\},$$

$$\vdots$$

$$\left\{\frac{-\lambda\alpha\sigma_{rr}^{0p(k+1)}}{n(1-\lambda)}\left[\left(\frac{r-R}{nh}\right)^{\lambda\alpha-1}-\left(\frac{r-R}{nh}\right)^{\alpha-1}\right]+\sigma_{rr}^{p(k+1)}\alpha\lambda\exp\left(-\alpha\lambda\left(\frac{r-R}{h}\right)\right)\right\}\left\{\frac{T_{k+1}}{h}+B_1^{(k+1)}\right\}$$

$$=\left\{\frac{-\lambda\alpha\sigma_{rr}^{0p(k)}}{n(1-\lambda)}\left[\left(\frac{r-R}{nh}\right)^{\lambda\alpha-1}-\left(\frac{r-R}{nh}\right)^{\alpha-1}\right]+\sigma_{rr}^{p(k)}\alpha\lambda\exp\left(-\alpha\lambda\left(\frac{r-R}{h}\right)\right)\right\}\{0+B_1^{(k)}\}.$$

From the above calculations we obtain

$$B_1^{(k)}=\frac{1}{\sigma_{rr}^{0p(k)}}\sum_{j=k+1}^{m}\sigma_{rr}^{0p(j)}\frac{T_j}{h}. \tag{19}$$

Similarly, the continuity conditions for σ_{zz} are:

$$0=\left\{\frac{\lambda\alpha\sigma_{rr}^{0p(m)}}{n^2(1-\lambda)}\left[(\lambda\alpha-1)\left(\frac{r-R}{nh}\right)^{\lambda\alpha-2}-(\alpha-1)\left(\frac{r-R}{nh}\right)^{\alpha-2}\right]+W_m\right\}\{0+0+B_2^{(m)}\}$$

$$\times\left\{\frac{\lambda\alpha\sigma_{rr}^{0p(m)}}{n^2(1-\lambda)}\left[(\lambda\alpha-1)\left(\frac{r-R}{nh}\right)^{\lambda\alpha-2}-(\alpha-1)\left(\frac{r-R}{nh}\right)^{\alpha-2}\right]+W_m\right\}\left\{\frac{1}{2}\left(\frac{T_m}{h}\right)^2+B_1^{(m)}\left(\frac{T_m}{h}\right)+B_2^{(m)}\right\}$$

$$=\left\{\frac{\lambda\alpha\sigma_{rr}^{0p(m-1)}}{n^2(1-\lambda)}\left[(\lambda\alpha-1)\left(\frac{r-R}{nh}\right)^{\lambda\alpha-2}-(\alpha-1)\left(\frac{r-R}{nh}\right)^{\alpha-2}\right]+W_{m-1}\right\}\{0+0+B_2^{(m-1)}\},$$

$$\vdots$$

$$\left\{\frac{\lambda\alpha\sigma_{rr}^{0p(k+1)}}{n^2(1-\lambda)}\left[(\lambda\alpha-1)\left(\frac{r-R}{nh}\right)^{\lambda\alpha-2}-(\alpha-1)\left(\frac{r-R}{nh}\right)^{\alpha-2}\right]+W_{k+1}\right\}$$

$$\times\left\{\frac{1}{2}\left(\frac{T_{k+1}}{h}\right)^2+B_1^{(k+1)}\left(\frac{T_{k+1}}{h}\right)+B_2^{(k+1)}\right\}$$

$$=\left\{\frac{\lambda\alpha\sigma_{rr}^{0p(k)}}{n^2(1-\lambda)}\left[(\lambda\alpha-1)\left(\frac{r-R}{nh}\right)^{\lambda\alpha-2}-(\alpha-1)\left(\frac{r-R}{nh}\right)^{\alpha-2}\right]+W_k\right\}\{0+0+B_2^{(k)}\}.$$

We have

$$B_2^{(k)}=\frac{1}{\sigma_{rr}^{0p(k)}}\left\{\sum_{j=k+1}^{m}\frac{1}{2}\left(\frac{T_j}{h}\right)^2\sigma_{rr}^{0p(j)}+\sum_{j=k+1}^{m}\frac{T_j}{h}\sigma_{rr}^{0p(j)}\sum_{i=k+1}^{j-1}\frac{T_i}{h}\right\}, \tag{20}$$

where

$$W_k=\sigma_{rr}^{p(k)}\alpha^2\lambda^2\exp\left(-\alpha\lambda\left(\frac{r-R}{h}\right)\right).$$

Then, the continuity conditions for $\sigma_{\theta z}$

$$0=\left\{\frac{-(\alpha-1)\sigma_{r\theta}^{0p(m)}}{n}\left(\frac{r-R}{nh}\right)^{\alpha-2}+\sigma_{r\theta}^{p(m)}\alpha\exp\left(-\alpha\left(\frac{r-R}{h}\right)\right)\right\}\{0+B_3^{(m)}\}$$

$$\times\left\{\frac{-(\alpha-1)\sigma_{r\theta}^{0p(m)}}{n}\left(\frac{r-R}{nh}\right)^{\alpha-2}+\sigma_{r\theta}^{p(m)}\alpha\exp\left(-\alpha\left(\frac{r-R}{h}\right)\right)\right\}\left\{\frac{T_m}{h}+B_3^{(m)}\right\}$$

$$= \left\{\frac{-(\alpha-1)\sigma_{r\theta}^{0p(m-1)}}{n}\left(\frac{r-R}{nh}\right)^{\alpha-2} + \sigma_{r\theta}^{p(m-1)}\alpha\exp\left(-\alpha\left(\frac{r-R}{h}\right)\right)\right\}\{0+B_3^{(m-1)}\},$$

$$\vdots$$

$$\left\{\frac{-(\alpha-1)\sigma_{r\theta}^{0p(k+1)}}{n}\left(\frac{r-R}{nh}\right)^{\alpha-2} + \sigma_{r\theta}^{p(k+1)}\alpha\exp\left(-\alpha\left(\frac{r-R}{h}\right)\right)\right\}\left\{\frac{T_{k+1}}{h}+B_3^{(k+1)}\right\}$$

$$= \left\{\frac{-(\alpha-1)\sigma_{r\theta}^{0p(k)}}{n}\left(\frac{r-R}{nh}\right)^{\alpha-2} + \sigma_{r\theta}^{p(k)}\alpha\exp\left(-\alpha\left(\frac{r-R}{h}\right)\right)\right\}\{0+B_3^{(k)}\}.$$

It yields

$$B_3^{(k)} = \frac{1}{\sigma_{r\theta}^{0p(k)}}\sum_{j=k+1}^{m}\sigma_{r\theta}^{0p(j)}\frac{T_j}{h}. \tag{21}$$

Thus $Q_{kl}^{(k)}(\eta)$ can be obtained by the substitution of eqns (19)–(21) into eqn (7), after arrangement they are

$$Q_{rz}^{(k)} = \frac{z}{h} + \frac{1}{\sigma_{rr}^{0p(k)}}\sum_{j=k+1}^{m}\sigma_{rr}^{0p(j)}\frac{T_j}{h},$$

$$Q_{\theta z}^{(k)} = \frac{z}{h} + \frac{1}{\sigma_{r\theta}^{0p(k)}}\sum_{j=k+1}^{m}\sigma_{r\theta}^{0p(j)}\frac{T_j}{h},$$

$$Q_{zz}^{(k)} = \frac{1}{2}\left(\frac{z}{h}\right)^2 + \left[\frac{1}{\sigma_{rr}^{0p(k)}}\sum_{j=k+1}^{m}\sigma_{rr}^{0p(j)}\frac{T_j}{h}\right]\left(\frac{z}{h}\right)$$

$$+ \left\{\frac{1}{\sigma_{rr}^{0p(k)}}\left[\sum_{j=k+1}^{m}\frac{1}{2}\left(\frac{T_j}{h}\right)^2\sigma_{rr}^{0p(j)} + \sum_{j=k+1}^{m}\frac{T_j}{h}\sigma_{rr}^{0p(j)}\sum_{i=k+1}^{j-1}\frac{T_i}{h}\right]\right\}. \tag{22}$$

The stresses in the kth ply can then be obtained by the functions $P_{kl}^{(k)}$ and $Q_{kl}^{(k)}$:

$$\sigma_{rr}^{0(k)} = \frac{\sigma_{rr}^{0p(k)}}{1-\lambda}\left[\left(\frac{r-R}{nh}\right)^{\lambda\alpha} - \lambda\left(\frac{r-R}{nh}\right)^{\alpha}\right] + \sigma_{rr}^{p(k)}\exp\left(-\alpha\lambda\left(\frac{r-R}{h}\right)\right),$$

$$\sigma_{r\theta}^{0(k)} = \sigma_{r\theta}^{0p(k)}\left(\frac{r-R}{nh}\right)^{\alpha-1} + \sigma_{r\theta}^{p(k)}\exp\left(-\alpha\left(\frac{r-R}{h}\right)\right),$$

$$\sigma_{rz}^{0(k)} = \left\{\frac{-\lambda\alpha}{n(1-\lambda)}\left[\left(\frac{r-R}{nh}\right)^{\lambda\alpha-1} - \left(\frac{r-R}{nh}\right)^{\alpha-1}\right] + \sigma_{rr}^{p(k)}\alpha\lambda\exp\left(-\alpha\lambda\left(\frac{r-R}{h}\right)\right)\right\}$$

$$\times\left[\sigma_{rr}^{0p(k)}\frac{z}{h} + \sum_{j=k+1}^{m}\sigma_{rr}^{0p(j)}t_j\right],$$

$$\sigma_{\theta z}^{0(k)} = \left\{\frac{-(\alpha-1)}{n}\left(\frac{r-R}{nh}\right)^{\alpha-2} + \sigma_{r\theta}^{p(k)}\alpha\exp\left(-\alpha\left(\frac{r-R}{h}\right)\right)\right\}\left[\sigma_{r\theta}^{0p(k)}\frac{z}{h} + \sum_{j=k+1}^{m}\sigma_{r\theta}^{0p(j)}t_j\right],$$

$$\sigma_{zz}^{0(k)} = \left\{\frac{\lambda\alpha}{n^2(1-\lambda)}\left[(\lambda\alpha-1)\left(\frac{r-R}{nh}\right)^{\lambda\alpha-2} - (\alpha-1)\left(\frac{r-R}{nh}\right)^{\alpha-2}\right] + \sigma_{rr}^{p(k)}\alpha^2\lambda^2\exp\left(-\alpha\lambda\left(\frac{r-R}{h}\right)\right)\right\}$$

$$\times\left\{\frac{1}{2}\sigma_{rr}^{0p(k)}\left(\frac{z}{h}\right)^2 + \left[\sum_{j=k+1}^{m}\sigma_{rr}^{0p(j)}t_j\right]\left(\frac{z}{h}\right) + \sum_{j=k+1}^{m}\frac{1}{2}t_j^2\sigma_{rr}^{0p(j)} + \sum_{j=k+1}^{m}t_j\sigma_{rr}^{0p(j)}\sum_{i=k+1}^{j-1}t_i\right\}. \tag{23}$$

Finally, stress function $\sigma_{\theta\theta}^{(k)}$ may be calculated from the strain–displacement and stress–strain relationships, that is

$$\sigma_{\theta\theta}^{(k)} = -(S_{12}\sigma_{rr}^{0(k)} + S_{13}\sigma_{zz}^{0(k)} - S_{16}\sigma_{r\theta}^{0(k)})/S_{11}. \tag{24}$$

3.3. *Determination of* α *and* λ

In order to evaluate the parameters of α and λ, two equations are required; the force resultants of both the exact plane stress and approximate three-dimensional solution in the boundary layer region must be equal, since both in-plane stress resultants must be in equilibrium with the corresponding resultant of the applied loading, thus

$$\int \sigma_{rr}^{p}\, dr = \frac{1}{h}\iint \sigma_{rr}^{0(k)}\, dr\, dz, \tag{25}$$

$$\int \sigma_{r\theta}^{p}\, dr = \frac{1}{h}\iint \sigma_{r\theta}^{0(k)}\, dr\, dz. \tag{26}$$

Then, the parameters of α and λ can be estimated by solving eqns (25) and (26) separately. The detailed procedure is given in Appendix B. Because the singular phenomenon of interlaminar stresses has been observed around the hole edge, the proper value of n which we previously used as the boundary layer range is selected such that the values of α and $\lambda\alpha$ satisfy the two inequalities:

$$1 < \alpha < 2, \tag{27}$$

$$1 < \lambda\alpha. \tag{28}$$

According to the above-mentioned analysis, we find that these out-of-plane stresses can be calculated from eqn (23). Therefore, this method of solution is very simple and the boundary-layer stress singularities in composite laminates with centrally circular holes are definitely evaluated.

4. NUMERICAL RESULTS AND DISCUSSIONS

Numerical results of three examples in graphite/epoxy laminates are due to the following elastic constants, ply thickness and hole radius:

$$E_{11} = 145\ \text{GPa}, \quad \nu_{12} = 0.31,$$

$$E_{22} = 10.7\ \text{GPa}, \quad \nu_{23} = 0.35,$$

$$G_{12} = G_{13} = 4.5\ \text{GPa}, \quad h = 4\ \text{mm}, \quad R = 8\ \text{mm}.$$

First, for a $[0/90]_S$ cross-ply laminate, six values of angle θ, namely, 15°, 30°, 45°, 60°, 75°, 85° are used, and the ratio of $(r-R)/h$ is assumed from 0.01 to n, not from 0 to n in order to avoid the singular properties of σ_{zz} and $\sigma_{\theta z}$ at $r = R$. The predicted in-plane normalized average stresses which compared with anisotropic elasticity solution by Savin

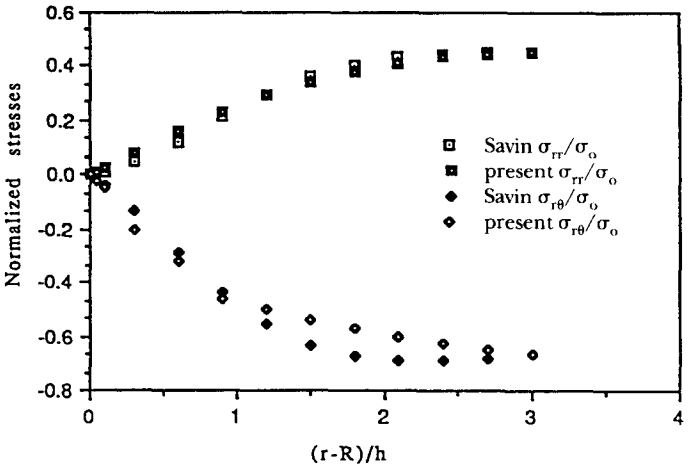

Fig. 2. Variation of in-plane stresses σ_{rr} and $\sigma_{r\theta}$ as a function of $(r-R)/h$ at $\theta = 30°$.

(1968) are shown in Fig. 2 at $\theta = 30°$ for example. The present solutions are found to be in very good agreement with Savin's solution for various angles along the hole edge. In the sequel figures of the in-plane stresses are all normalized.

Figure 3 shows σ_{rr}/σ_0 and $\sigma_{r\theta}/\sigma_0$ around the hole at a distance of one eighth of the radius from the edge, σ_{rr}/σ_0 compared well with Savin (1968) and $\sigma_{r\theta}/\sigma_0$ is slightly different from that by Savin (1968). Figure 4 illustrates the results in very good agreement with those by Savin for $\sigma_{r\theta}$ and σ_{rr} around the hole at a distance of half the radius from the hole edge. In comparison with the numerical predictions of Figs 3 and 4, we obviously observe that at a distance far away from the hole edge, both the results of our method and Savin's are becoming close to each other for in-plane stresses. However, it should be noted that for a three-dimensional solution in an area, very close to the hole edge, the in-plane stresses are not expected to agree very well with the two-dimensional solution by Savin (1968), since the singularity affects the interlaminar stresses significantly.

Figure 5 represents the distributions of interlaminar stresses σ_{zz} and $\sigma_{\theta z}$ around the hole. $\sigma_{\theta z}/\sigma_0$ has a very similar shape of stress behavior to that of Zhang and Ueng (1988), especially for $\theta = 25$–$45°$ at a distance of $(r-R)/h = 0.01$ from the hole edge, and also very close to these values by Zhang and Ueng (1988) for the specific angle and distance. The obtained peak value of $\sigma_{\theta z}/\sigma_0$ is 0.75, while that of Zhang and Ueng (1988) is 0.8. Similarly,

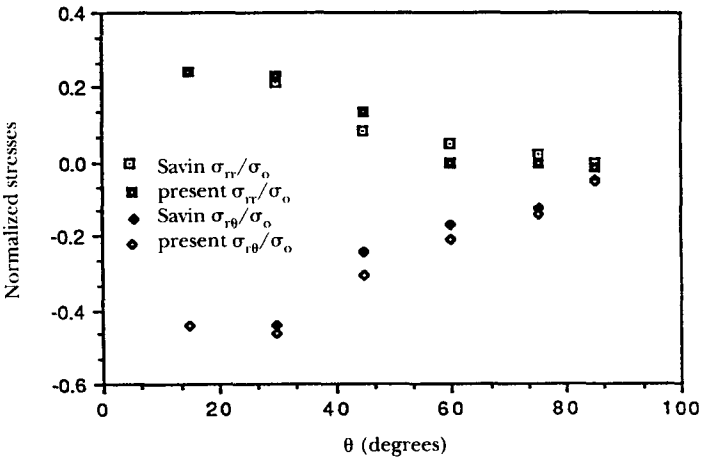

Fig. 3. Variation of in-plane stresses σ_{rr} and $\sigma_{r\theta}$ around the hole at $r-R = R/8$.

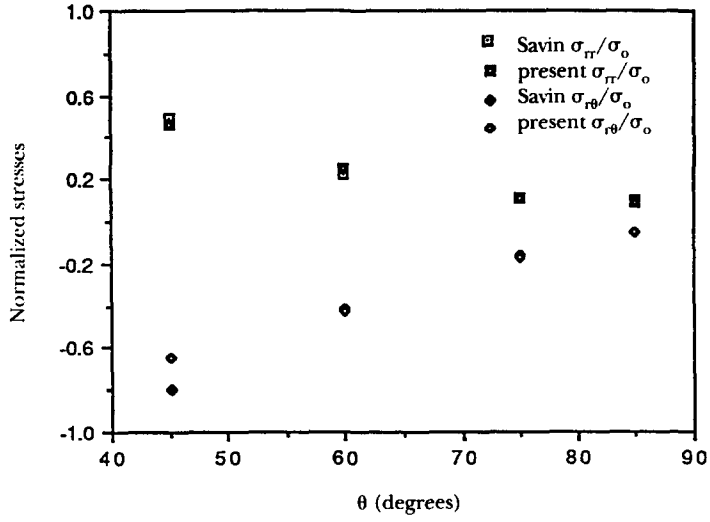

Fig. 4. Variation of in-plane stresses σ_{rr} and $\sigma_{r\theta}$ around the hole at $r-R = R/2$.

the presented and referred curves of σ_{zz}/σ_0 are close to each other too, in addition the peak value we obtained is 0.24 while that of Zhang and Ueng (1988) is 0.2.

It is now well known that the rapidly varying interlaminar stresses are found near the free edge of a laminated composite. Based on eqns (26) and (27), the order of singularity can be solved in our model. For illustration, the singularity for the free edge of a $[0/90]_s$ graphite/epoxy laminate around a quarter circular hole is shown in Fig. 6. The values of singularity must be positive, since the inequality relations in eqn (28) need to be satisfied. The order of singularity provides us with the important information to predict the initiation of delamination.

The overall distribution of $\sigma_{\theta z}$ compares well with the curve by Zhang and Ueng (1988) except for a small range of angles over 70° where $\sigma_{\theta z}$ is small but negative. This weakness can be improved by a slight modification of selecting more suitable functions.

Additionally, Figs 7–9 provide more evidence that the interlaminar stresses are very close to those by Zhang and Ueng (1988) at the specific angle $\theta = 81°$ and ratio $R/h = 100$. Figure 7 presents the profile of interlaminar normal stress σ_{zz}/σ_0. We find that both curves fit well for $(r-R)/2h$ larger than 0.5. Figure 8 depicts the interlaminar shear stress $\sigma_{\theta z}/\sigma_0$. These values possess a singularity near the hole edge, and diminish quickly at a distance of

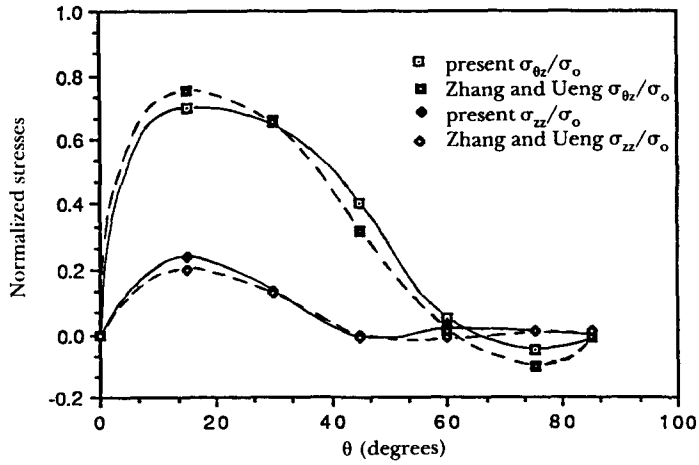

Fig. 5. Variation of interlaminar stresses around the hole edge at $(r-R)/h = 0.01$.

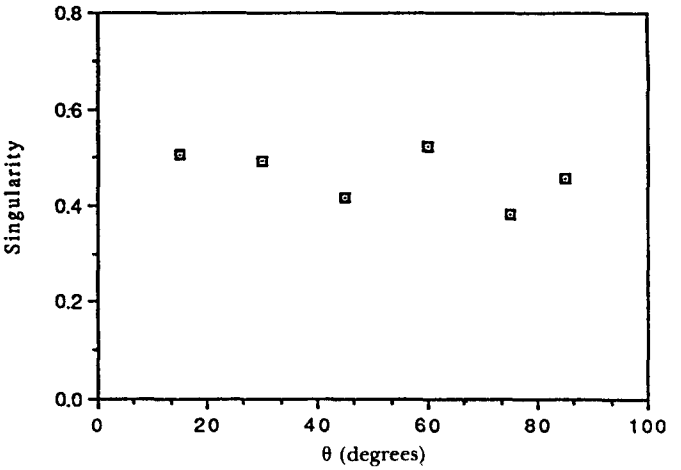

Fig. 6. Singularity of a [0/90]$_s$ graphite/epoxy laminate around a quarter circular hole.

about one ply thickness. Although our results are always lower than those by Zhang and Ueng (1988), they agree very well with each other. The distribution of interlaminar shear stress σ_{rz}/σ_0 is described in Fig. 9, the general trend agrees very well and the results are quite close to each other.

Figures 10–12 are the predictions plotted for $[\pm 45]_s$ laminates compared to Tang (1977) with the following material properties:

$$E_{11} = 137\ \text{GPa}, \quad E_{22} = E_{33} = 14.4\ \text{GPa},$$
$$G_{12} = G_{13} = G_{23} = 5.85\ \text{GPa},$$
$$\nu_{12} = \nu_{13} = \nu_{23} = 0.21, \quad h = 4\ \text{mm}, \quad R = 400\ \text{mm}.$$

Figure 10 presents the interlaminar shear stress $\sigma_{\theta z}/\sigma_0$ from the hole edge at $\theta = 0°$ with $R/h = 100$. The stress increases rapidly toward the hole edge because of singular effect, but it is close to zero and becomes smooth for $(r-R)/2h > 0.5$. Interlaminar normal stress

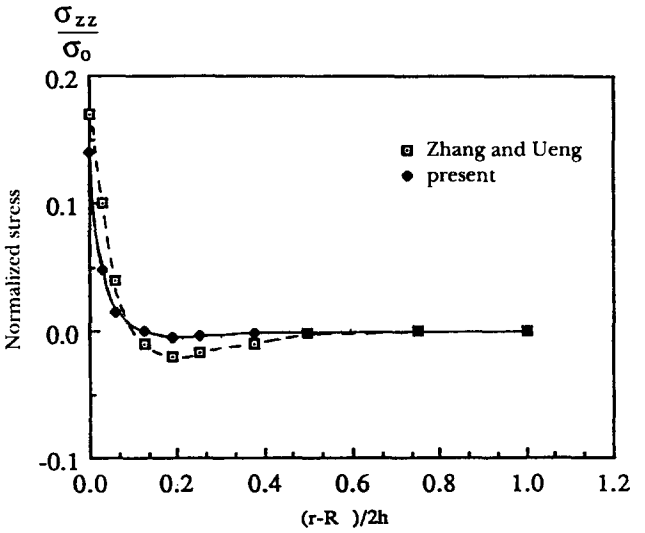

Fig. 7. Distribution of σ_{zz}/σ_0 for [0/90]$_s$ laminate under uniaxial tension at $\theta = 81°$ for ratio $R/h = 100$.

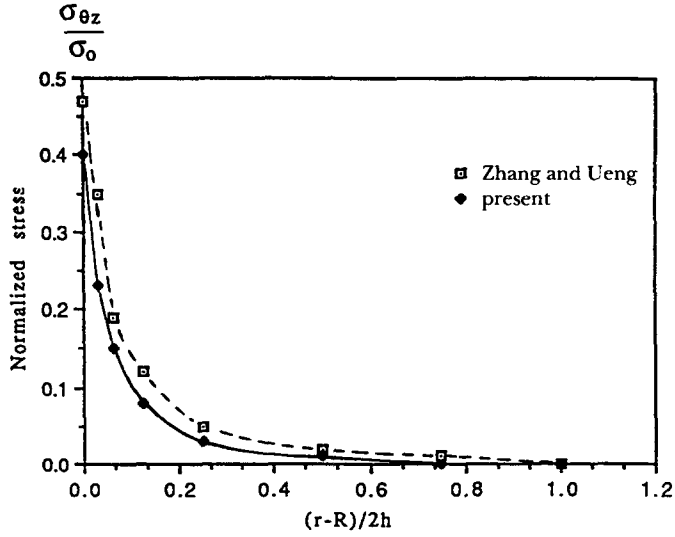

Fig. 8. Distribution of $\sigma_{\theta z}/\sigma_0$ for $[0/90]_s$ laminate under uniaxial tension at $\theta = 81°$ for ratio $R/h = 100$.

σ_{zz}/σ_0 is illustrated in Fig. 11 for the same angle and ratio. The general trend follows well, especially in the regions near and far from the hole edge. The only difference is that the minimum value in the central portion is negative and higher than that by Tang (1977), but actually it does not have much effect on delamination. Figure 12 shows the interlaminar shear stress σ_{rz}/σ_0 from the hole edge at $\theta = 0°$, they compare very well except at the hole edge. However, the value of σ_{rz} is generally much smaller than other interlaminar stresses, so it does not have much effect from a practical point of view.

Finally, Fig. 13 summarizes the interlaminar stresses around the circular hole in the $[0/90/\pm 45]_s$ laminate at the midplane. We use the same material properties as those in the $[0/90]_s$ laminate with the ratio of thickness to radius equal to 1/10. Without repetition of plotting the stress profiles as shown in $[0/90]_s$ and $[\pm 45]_s$ for specific conditions, it is seen that the interlaminar shear stress $\sigma_{\theta z}$ is the dominating component and has the maximum value at about 50° from the loading direction. The other two components of interlaminar

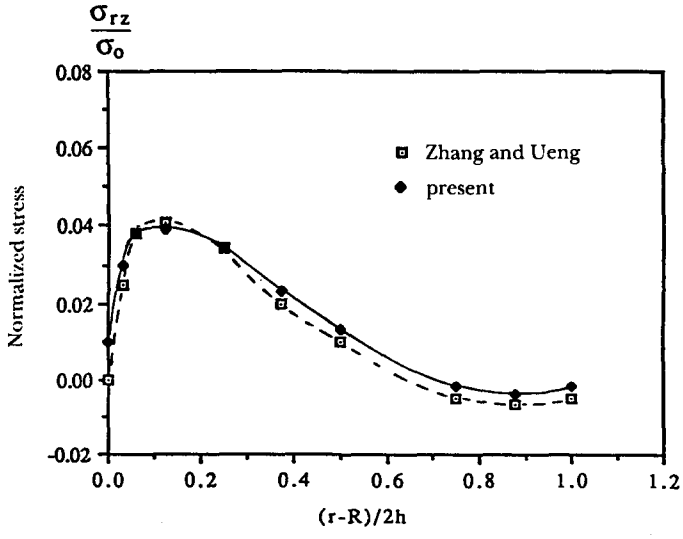

Fig. 9. Distribution of σ_{rz}/σ_0 for $[0/90]_s$ laminate under uniaxial tension at $\theta = 81°$ for ratio $R/h = 100$.

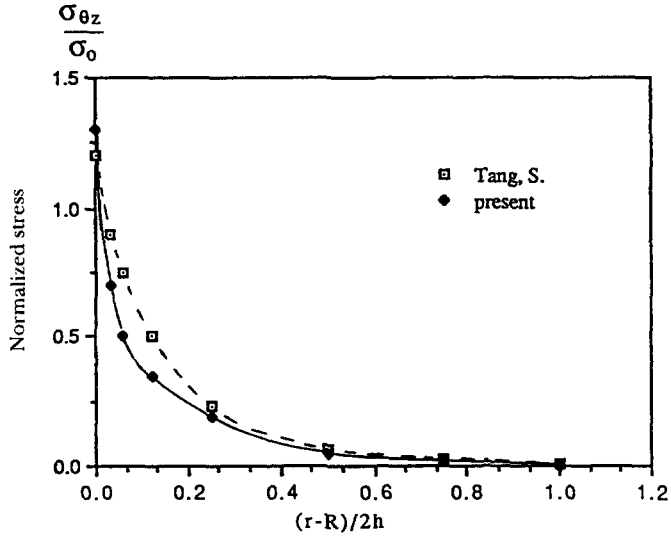

Fig. 10. Distribution of $\sigma_{\theta z}/\sigma_0$ for $[\pm 45]_s$ laminate under uniaxial tension at $\theta = 0°$ for ratio $R/h = 100$.

stresses σ_{zz} and $\sigma_{\theta z}$ are comparatively small. The computing time of each case on a CDC system is listed in Table 1 for reference. We find that the CPU time is less than half a minute even for the thickness of 48 plies. Hence, our approach is verified to be a simple and efficient one.

5. CONCLUSIONS

In order to obtain reasonably accurate approximate interlaminar stresses in a composite laminate with a centrally circular hole, the method of analysis is proposed herein using matched asymptotic expansions by Tang (1977). The solution is derived and obtained by the combination of interior in-plane stress and boundary layer stress fields. A computer code in FORTRAN incorporating the present method is adopted to conduct the various manipulations of mathematical operations in a CDC computer system. The merits of the

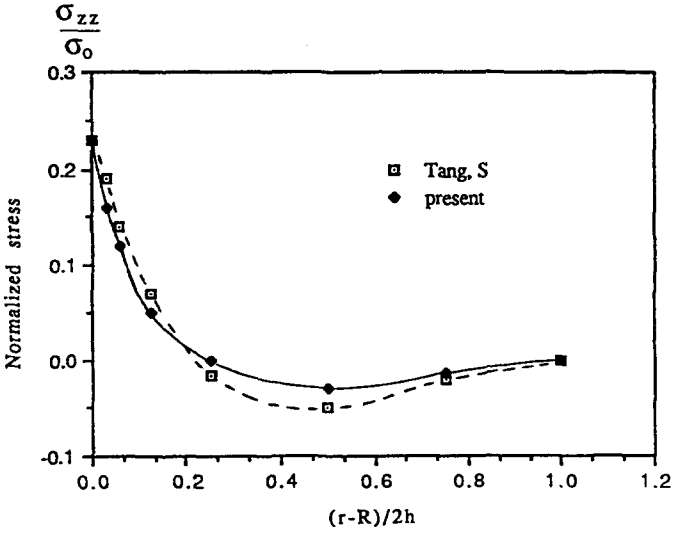

Fig. 11. Distribution of σ_{zz}/σ_0 for $[\pm 45]_s$ laminate under uniaxial tension at $\theta = 0°$ for ratio $R/h = 100$.

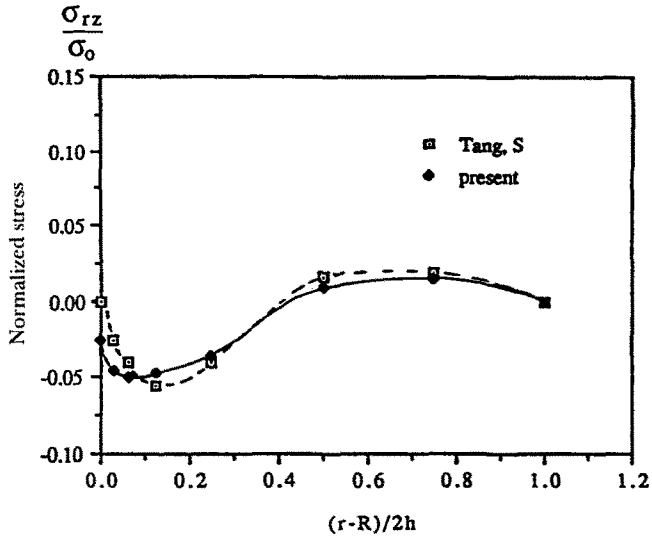

Fig. 12. Distribution of σ_{rz}/σ_0 for $[\pm 45]_s$ laminate under uniaxial tension at $\theta = 0°$ for ratio $R/h = 100$.

proposed method are simple and efficient. The analytical predictions, including the value of singularity, are in good agreement with those stated in the literature. From our work the following concluding remarks would be pertinent:

(1) The interlaminar stresses in centrally notched composite laminates are obtained;

(2) Their respectively singularities come simultaneously;

(3) The proposed method is simple and suitable for engineering applications, especially in the preliminary design stage.

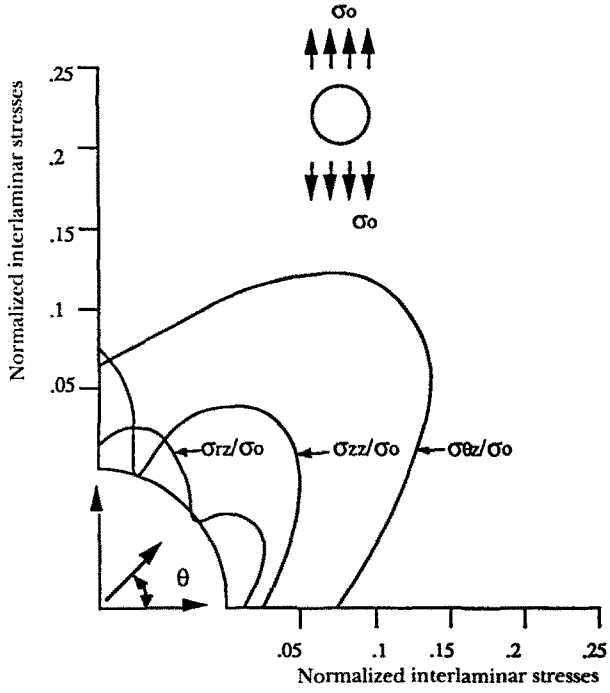

Fig. 13. Variation of interlaminar stresses around the hole in $[0/90/\pm 45]_s$ laminate at midplane.

Table 1. Computer execution time for various laminates

Laminate	R/h	CPU (seconds)
$[\pm 45]_s$	100	1.5
$[\pm 45]_{2s}$	50	2.01
$[\pm 45]_{4s}$	25	3.25
$[\pm 45]_{8s}$	12.5	6.05
$[\pm 45]_{24s}$	4.2	25.5
$[0/90]_s$	100	1.5
$[0/90]_{2s}$	50	2.0
$[0/90]_{4s}$	25	3.2
$[0/90]_{8s}$	12.5	6.0
$[0/90]_{24s}$	4.2	25.0

Acknowledgements—The authors are grateful for the support and assistance of the project (NSC 79-0401-E110-09) sponsored by the National Science Council, ROC. The first author would also like to take the opportunity to thank Dr K. L. Reifsnider for his kind instructions at VPI & SU.

REFERENCES

Carlsson, L. (1983). Interlaminar stresses at a hole in a composite member subjected to in-plane loading. *J. Compos. Mater.* **17,** 238–249.

Ericson, K., Persson, M., Carlsson, L. and Gustavsson, A. (1984). On the prediction of the initiation of delamination in a $[0/90]_s$ laminates with a circular hole. *J. Compos. Mater.* **18,** 495–506.

Jen, M.-H. R., Hsu, J. M., Kau, Y. S. and Kao, P. W. (1992). The interlaminar stresses at straight edges in composite laminates. *J. Reinforced Plastics and Compos.* **11**(6), 584–599.

Kassapoglou, C. and Lagace, P. A. (1986). An efficient method for the calculation of interlaminar stresses in composite materials. *J. Appl. Mech.* **53,** 744–750.

Lekhnitskii, S. G. (1963). *Theory of Elasticity of an Anisotropic Body*. Holden Day, San Francisco.

Lekhnitskii, S. G. (1968). *Anisotropic Plates*. Gordon & Breach, New York.

Lucking, W. M., Itoa, S. V. and Sankar, T. S. (1984). The effect of geometry on interlaminar stresses of $[0/90]_s$ composite laminates with circular holes. *J. Compos. Mater.* **17,** 188–198.

Pipes, R. B. and Pagano, N. J. (1970). Interlaminar stresses in composite materials under uniform axial extension. *J. Compos. Mater.* **4,** 538–548.

Reiss, E. L. (1961). Extension of a thick infinite plate with a circular hole. Report of New York University IMM-NYU-281.

Rybicki, E. F. and Schmueser, D. W. (1976). Three-dimensional finite element stress analysis of laminated plates containing a circular hole. Battelle, Columbus Laboratories, Columbus, Ohio, AFML-TR-76-92.

Savin, G. N. (1968). Stress distribution around holes. NASA TT F-607.

Spilker, R. L. and Chou, S. C. (1980). Edge in symmetric composite laminates: importance of satisfying the traction-free-edge condition. *J. Compos. Mater.* **14,** 2–20.

Tang, S. (1977). Interlaminar stresses around circular cutouts in composite plates under tension. *AIAA Jl* **15,** 1631–1637.

Timoshenko, S. P. and Goodier, J. N. (1951). *Theory of Elasticity*. McGraw-Hill, New York.

Wang, A. S. D. and Crossman, F. W. (1977). Some new results on edge effect in symmetric composite laminates. *J. Compos. Mater.* **11,** 92–106.

Wang, S. S. and Choi, I. (1982a). Boundary-layer effects in composite laminates: Part I—Free edge stress singularities. *J. Appl. Mech.* **49,** 541–548.

Wang, S. S. and Choi, I. (1982b). Boundary-layer effects in composite laminates: Part II—Free edge stress solutions and basic characteristics. *J. Appl. Mech.* **49,** 549–560.

Ye, L. and Yang, B.-X. (1988). A boundary layer approach to interlaminar stresses in composite laminates with curved edges. *J. Reinforced Plastic and Compos.* **7,** 179–198.

Zhang, K.-D. and Ueng, C. E. S. (1988). A simplified approach for interlaminar stresses around a hole in $[0/90]_s$ laminates. *J. Compos. Mater.* **22,** 192–202.

APPENDIX A

The plane stress constitutive equation

$$\begin{bmatrix} \sigma_{xx} \\ \sigma_{yy} \\ \sigma_{xy} \end{bmatrix}^{(k)} = \begin{bmatrix} Q_{11}Q_{12}Q_{16} \\ Q_{12}Q_{22}Q_{26} \\ Q_{16}Q_{26}Q_{66} \end{bmatrix}^{(k)} \begin{bmatrix} \varepsilon_{xx} \\ \varepsilon_{yy} \\ \varepsilon_{xy} \end{bmatrix},$$

where

$$Q_{ij} = C_{ij} - \frac{C_{i3}C_{j3}}{C_{33}}.$$

For a material having transverse isotropy relative to the x_2–x_3 plane, we find

$$C'_{11} = (1-\nu_{23}^2)\frac{E_{11}}{V},$$

$$C'_{13} = C'_{12} = \nu_{12}(1+\nu_{23})\frac{E_{22}}{V},$$

$$C'_{23} = \left(\nu_{23}+\nu_{12}^2\frac{E_{22}}{E_{11}}\right)\frac{E_{22}}{V},$$

$$C'_{33} = C'_{22} = \left(1-\nu_{12}^2\frac{E_{22}}{E_{11}}\right)\frac{E_{22}}{V},$$

$$C'_{44} = G_{23} = \frac{E_{22}}{2(1+\nu_{23})},$$

$$C'_{55} = C'_{66} = G_{12},$$

where

$$V = \left[(1+\nu_{23})\left(1-\nu_{23}-2\nu_{12}^2\frac{E_{22}}{E_{11}}\right)\right].$$

Stiffness transformation equations for an orthotropic C' matrix:

$$C_{11} = C'_{11}m^4+2(C'_{12}+2C'_{66})m^2n^2+C'_{22}n^4,$$
$$C_{12} = (C'_{11}+C'_{22}-4C'_{66})m^2n^2+C'_{12}(m^4+n^4),$$
$$C_{13} = C'_{13}m^2+C'_{23}n^2,$$
$$C_{16} = [C'_{11}m^2-C'_{22}n^2-(C'_{12}+2C'_{66})(m^2-n^2)]mn,$$
$$C_{22} = C'_{11}n^4+2(C'_{12}+2C'_{66})m^2n^2+C'_{22}m^4,$$
$$C_{23} = C'_{13}n^2+C'_{23}m^2,$$
$$C_{26} = [C'_{11}n^2-C'_{22}m^2+(C'_{12}+2C'_{66})(m^2-n^2)]mn,$$
$$C_{33} = C'_{33},$$
$$C_{36} = (C'_{23}-C'_{13})mn,$$
$$C_{44} = C'_{44}m^2+C'_{55}n^2,$$
$$C_{45} = (C'_{44}-C'_{55})mn,$$
$$C_{55} = C'_{44}n^2+C'_{55}m^2,$$
$$C_{66} = (C'_{11}+C'_{22}-2C'_{12})m^2n^2+C'_{66}(m^2-n^2)^2,$$
$$C_{14} = C_{15} = C_{24} = C_{25} = C_{34} = C_{35} = C_{46} = C_{56} = 0,$$

where $m = \cos\theta$, $n = \sin\theta$.

Note that the transformed matrix $[C]$, is no longer orthotropic. The elements of the stiffness matrix

$$a_{ij} = \frac{1}{h}\int_{-h/2}^{h/2} Q_{ij}^{(k)}\,dz = \sum Q_{ij}^{(k)}\frac{T_k}{h}, \quad i,j = 1,2,6.$$

The elements of the flexibility matrix

$$[b_{ij}] = [a_{ij}]^{-1}$$
$$\therefore \varepsilon_i = b_{ij}\sigma_j.$$

APPENDIX B

$$\sigma_{rr} = \sigma_{yy}\cos^2\theta+\sigma_{xx}\sin^2\theta+2\sigma_{xy}\sin\theta\cos\theta,$$
$$\sigma_{r\theta} = (\sigma_{xx}-\sigma_{yy})\sin\theta\cos\theta+\sigma_{xy}(\cos^2\theta-\sin^2\theta),$$
$$\therefore \sigma_{rr}^p = \{\sigma_0+2\,\mathrm{Re}\,[\mu_1^2\phi'_1(z_1)+\mu_2^2\phi'_2(z_2)]\}\sin^2\theta+\{2\,\mathrm{Re}\,[\phi'_1(z_1)+\phi'_2(z_2)]\}\cos^2\theta$$
$$+2\{-2\,\mathrm{Re}\,[\mu_1\phi'_1(z_1)+\mu_2\phi'_2(z_2)]\}\sin\theta\cos\theta,$$
$$\sigma_{r\theta}^p = \{\sigma_0+2\,\mathrm{Re}\,[(\mu_1^2-1)\phi'_1(z_1)+(\mu_2^2-1)\phi'_2(z_2)]\}\sin\theta\cos\theta+\{-2\,\mathrm{Re}\,[\mu_1\phi'_1(z_1)+\mu_2\phi'_2(z_2)]\}(\cos^2\theta-\sin^2\theta),$$

where

$$z_i = x+\mu_i y = r(\sin\theta+\mu_i\cos\theta), \qquad i=1,2,$$

$$\phi_j'(z_j) = \phi_j'(r)\frac{\mathrm{d}r}{\mathrm{d}z_j} = \phi_j'(r)/(\sin\theta+\mu_j\cos\theta), \quad j=1,2,$$

$$\int_R^{R+nh}\sigma_{rr}^{\mathrm{p}}\,\mathrm{d}r = \left\{\sigma_0 nh+2\,\mathrm{Re}\left[\frac{\mu_1^2[\phi_1(R+nh)-\phi_1(R)]}{\sin\theta+\mu_1\cos\theta}+\frac{\mu_2^2[\phi_2(R+nh)-\phi_2(R)]}{\sin\theta+\mu_2\cos\theta}\right]\right\}$$
$$\times\sin^2\theta+\left\{2\,\mathrm{Re}\left[\frac{\phi_1(R+nh)-\phi_1(R)}{\sin\theta+\mu_1\cos\theta}+\frac{\phi_2(R+nh)-\phi_2(R)}{\sin\theta+\mu_2\cos\theta}\right]\right\}\cos^2\theta$$
$$+2\left\{-2\,\mathrm{Re}\left[\frac{\mu_1[\phi_1(R+nh)-\phi_1(R)]}{\sin\theta+\mu_1\cos\theta}+\frac{\mu_2[\phi_2(R+nh)-\phi_2(R)]}{\sin\theta+\mu_2\cos\theta}\right]\right\}\sin\theta\cos\theta,$$

$$\frac{1}{h}\int_{-h/2}^{h/2}\int_R^{R+nh}\sigma_{rr}^{0(k)}\,\mathrm{d}r\,\mathrm{d}z = \frac{\sigma_{rr}^{0\mathrm{p}}}{1-\lambda}\left[\frac{nh}{\lambda\alpha+1}-\frac{\lambda nh}{\alpha+1}\right],$$

$$\int_R^{R+nh}\sigma_{r\theta}^{\mathrm{p}}\,\mathrm{d}r = \left\{\sigma_0 nh+2\,\mathrm{Re}\left[\frac{(\mu_1^2-1)[\phi_1(R+nh)-\phi_1(R)]}{\sin\theta+\mu_1\cos\theta}+\frac{(\mu_2^2-1)[\phi_2(R+nh)-\phi_2(R)]}{\sin\theta+\mu_2\cos\theta}\right]\right\}\sin\theta\cos\theta$$
$$+\left\{-2\,\mathrm{Re}\left[\frac{\mu_1[\phi_1(R+nh)-\phi_1(R)]}{\sin\theta+\mu_1\cos\theta}+\frac{\mu_2[\phi_2(R+nh)-\phi_2(R)]}{\sin\theta+\mu_2\cos\theta}\right]\right\}(\cos^2\theta-\sin^2\theta),$$

$$\frac{1}{h}\int_{-h/2}^{h/2}\int_R^{R+nh}\sigma_{r\theta}^{0(k)}\,\mathrm{d}r\,\mathrm{d}z = \frac{\sigma_{r\theta}^{0\mathrm{p}}nh}{\alpha}.$$